Environmental Science and Ecotechnology 21 (2024) 100394

Contents lists available at ScienceDirect

Environmental Science and Ecotechnology

journal homepage: www.journals.elsevier.com/environmental-science-and-ecotechnology/

Original Research

Crop residue burning in China (2019–2021): Spatiotemporal patterns, environmental impact, and emission dynamics

Qiancheng Lv [a], Zeyu Yang [a], Ziyue Chen [a, *], Manchun Li [b], Bingbo Gao [c], Jing Yang [a], Xiao Chen [a], Bing Xu [d, **]

[a] Faculty of Geographical Science, Beijing Normal University, Beijing, 100875, China
[b] School of Geography and Ocean Science, Nanjing University, Nanjing, 210023, China
[c] College of Land Science and Technology, China Agriculture University, Beijing, 100083, China
[d] Department of Earth System Science, Tsinghua University, Beijing, 100084, China

ARTICLE INFO

Article history:
Received 3 July 2023
Received in revised form
17 January 2024
Accepted 19 January 2024

Keywords:
Crop residue burning
Atmospheric pollutants
NSMC-Himawari-8
Lagging effects

ABSTRACT

Crop residue burning (CRB) is a major contributor to air pollution in China. Current fire detection methods, however, are limited by either temporal resolution or accuracy, hindering the analysis of CRB's diurnal characteristics. Here we explore the diurnal spatiotemporal patterns and environmental impacts of CRB in China from 2019 to 2021 using the recently released NSMC-Himawari-8 hourly fire product. Our analysis identifies a decreasing directionality in CRB distribution in the Northeast and a notable southward shift of the CRB center, especially in winter, averaging an annual southward movement of 7.5°. Additionally, we observe a pronounced skewed distribution in daily CRB, predominantly between 17:00 and 20:00. Notably, nighttime CRB in China for the years 2019, 2020, and 2021 accounted for 51.9%, 48.5%, and 38.0% respectively, underscoring its significant environmental impact. The study further quantifies the hourly emissions from CRB in China over this period, with total emissions of CO, PM_{10}, and $PM_{2.5}$ amounting to 12,236, 2,530, and 2,258 Gg, respectively. Our findings also reveal variable lag effects of CRB on regional air quality and pollutants across different seasons, with the strongest impacts in spring and more immediate effects in late autumn. This research provides valuable insights for the regulation and control of diurnal CRB before and after large-scale agricultural activities in China, as well as the associated haze and other pollution weather conditions it causes.

1. Introduction

Crop residue burning (CRB) is considered the fourth largest type of biomass combustion worldwide and a significant source of air pollutants (including gaseous pollutants and particulate matter) and greenhouse gases [1–3], which poses a serious threat to air quality [4,5] and climate change [6–8]. More importantly, toxicological studies revealed that compared with aerosols generated from fossil fuels, pollution particles emitted from biomass presented greater toxicity [8]. Meanwhile, pollutants emitted by CRB present notable lagging effects and may last for days, causing long-term impacts on local air quality and the public's exposure risk [9]. In this case, airborne pollutants from CRB increase local mortality rates and pose substantial threats to public health through direct and indict means [10–12]. For instance, from 2003 to 2019, CRB caused 44,000–98,000 particulate matter exposure-related premature deaths and a total loss of 3.2 billion US dollars in India [13]. A study from China revealed that a 10 μg m^{-3} increase in $PM_{2.5}$ emitted by CRB increases monthly mortality by 3.25% [14].

As the world's largest grain-producing and crop residue surplus country [11,15,16], CRB has become one major approach to processing crop residues in China. With the release of the national "Clean Air" action in 2013, specific regulations have been released to reduce CRB. Nevertheless, CRB spots continued to rise annually until 2015 [17]. With a stricter implementation of regulation measures, the prevalence of CRB in China declined significantly in recent years [18], yet massive CRB remained, resulting in the discharge of megatons of airborne pollutants into the atmosphere

* Corresponding author.
** Corresponding author.
E-mail addresses: zychen@bnu.edu.cn (Z. Chen), bingxu@tsinghua.edu.cn (B. Xu).

https://doi.org/10.1016/j.ese.2024.100394

[9]. To better understand the characteristics of CRB and implement regulation measures accordingly, increasing studies have been conducted on the spatiotemporal distribution [19] and environmental effects [20] of CRB in China.

Despite an improved understanding of CRB in China, major limitations remained. The monitoring of CRB is mainly realized based on a diversity of remote sensing data, the efficiency and reliability of which are subject to the spatiotemporal resolution and accuracy of the data sources employed. Currently, the commonly employed active fire products that can be used for monitoring CRB in China include VIIRS (Visible Infrared Imaging Radiometer Suite) daily, MODIS (Moderate-Resolution Imaging Spectroradiometer) daily, and JMA-Himawari-8 hourly fire products. Specially, VIIRS fire products are of the highest spatial resolution (375 m), so it has a strong capability for capturing small-scale fires [21]. MODIS fire products presented a long-time series and are thus widely employed for investigating long-term variations of CRB. However, as we know, CRB lasts a relatively short period, ranging from minutes to hours [22]. Therefore, the daily frequency leads to massive missed identification of fires. Since the passing time for both VIIRS and MODIS in China is around 10:30 and 13:30, nighttime CRB cannot be detected, causing a largely biased understanding of CRB in China. Farmers in China used to burn crop residues in the daytime. After the release of CRB-related regulations, nighttime CRB has increased dramatically [23]. Currently, the JMA-Himawari-8 is the sole hourly fire product available. Yet, this product is compromised by a large amount of false fire information and holds a low overall accuracy in China [24,25]. Consequently, this limitation hinders a comprehensive analysis of the diurnal characteristics of CRB in China.

In addition to the difficulty in accurately identifying CRB, calculating the pollutant emissions from CRB is also subject to many limitations. Traditional methods for estimating pollutant emissions from CRB mainly rely on statistical and survey data [26,27]. These approaches involve multiple statistical data, such as crop yields and conversion rates, with specific Emission Factors (EFs) to estimate emissions of different pollutants [28]. While reliable under conditions of abundant data, these approaches face several limitations. Firstly, it requires a substantial amount of manpower, material resources, and financial resources to collect the necessary reference data. Secondly, regions usually employ different statistical indicators, challenging data integration [29]. Thirdly, the delayed release of field-collected statistics, often by 1–5 years, limits the timeliness and relevance of the data [30]. Advances in satellite observation have provided an alternative approach for real-time estimation of CRB pollutant emissions. A widely adopted strategy involves estimating emissions based on satellite-derived fire radiative energy (FRE) [31,32]. However, due to different agricultural planting areas in China, using one fixed EFs to estimate CRB pollutant emissions nationwide can cause significant errors [33,34].

To address this issue, we employed our recently released hourly NSMC-Himawari-8 fire product [25], offering superior spatial and temporal resolution and enhanced accuracy compared to the JMA-Himawari-8 product. This approach was adopted to deepen our understanding of China's CRB, especially the inter-annual variations of daytime and nighttime CRB and its potential environmental effects. Firstly, we revealed the spatial distribution of CRB in China between 2019 and 2021 at seasonal and diurnal scales. Next, a method based on FRE and regional EFs was employed to estimate the emissions of three major pollutants (CO, $PM_{2.5}$, and PM_{10}), focusing on the differences between daytime and nighttime emissions. Finally, we analyzed the lagging effects of CRB on the regional air quality. This research provides a new vision to evaluate the spatiotemporal variations of daytime and nighttime CRB in China and sheds light on better monitoring CRB and implementing management measures accordingly.

2. Data and methodology

2.1. Data sources

2.1.1. NSMC-Himawari-8 hourly fire product

NSMC-Himawari-8 hourly fire product (https://doi.org/10.6084/m9.figshare.21550248) was released specifically to better identify fires in China. Based on the original Himawari-8 satellite data (https://www.eorc.jaxa.jp/ptree/), this fire product employed dynamic fire-identification thresholds, more effectively identifying fire spots in China. Furthermore, according to two specific ground thermal-source databases, most false fire pixels in the JMA-Himawari-8 were effectively removed. Therefore, the overall accuracy for NSMC-Himawari-8 hourly fire products in China reached 80%, much higher than the original JMA-Himawari-8 fire product (54%). If those omission errors caused by the system resolution limitations were not considered, the overall accuracy for the NSMC-Himawari-8 hourly fire product reached 84%, compared with 59% for the JMA-Himawari-8 fire product. The NSMC-Himawari-8 fire product is advantageous in its hourly temporal resolution, facilitating continuous daytime and nighttime detection of CRB. The spatial resolution for the NSMC-Himawari-8 fire product is 0.02°, providing fire information such as geographic location, fire area, fire radiative power (FRP), and the number of fire pixels. To extract CRB pixels from the entire fire sets, we utilized an underlying surface file from Land cover classification gridded maps (ESA Climate Change Initiative, https://doi.org/10.24381/cds.006f2c9a). This map includes several surface types, such as cropland, tree cover, and grassland, and boasts an overall accuracy of 90%. It served as a farmland mask to clip CRB pixels from overall fire pixels. Since Himawari-8 fire data were available in late 2018, this research employed NSMC-Himawari-8 fire products from 2019 to 2021 to extract hourly CRB pixels across China.

2.1.2. Airborne pollutant data

The CHAP dataset (https://weijing-rs.github.io/product.html) was used to investigate the lagging effect of CRB on air quality. CHAP, which is generated from big data (e.g., ground measurements, satellite remote sensing products), atmospheric reanalysis, model simulations, and artificial intelligence, offers long-term, fully covered, and high-resolution information on the spatiotemporal heterogeneity of multiple airborne pollutants [35]. For this study, we collected daily concentration data on CO, $PM_{2.5}$, and PM_{10} with a spatial resolution of 10 km and respective cross-validation coefficients (CV-R2) of 0.80, 0.90, and 0.86 [36].

2.2. Methodology

2.2.1. Spatiotemporal distribution of CRB

To reveal the density distribution of CRB during different seasons from 2019 to 2021, we established a fishing net with a size of $0.2° \times 0.2°$ covering the entirety of China. Next, to comprehensively analyze the spatiotemporal variations in the distribution of CRB from 2019 to 2021, we employed standard deviation ellipse (SDE) and median center (MEC) analysis. SDE is commonly used to analyze the spatial distribution and range changes of fire spots [37]. MEC is an iterative algorithm used to determine the center position of spatially dense phenomena [38], such as fire spots in this research (details of SDE and MEC are seen in Text S1 in Supplementary Materials).

2.2.2. Estimation of CRB emissions

Inspired by previous studies [39] we addressed this issue by dividing the country into seven regions according to geographical location, crop types, and biomass-burning characteristics. Adopting unique pollutant EFs for each region can largely avoid the estimation uncertainties.

We followed the method proposed by Xu et al. (2022) [39] and used the equation (1) to calculate the CRB emissions based on the EFs of three pollutants and FRE:

$$E_i = \sum_{j,t,m} (FRE_{j,t,m} \times EF_{i,j}) \quad (1)$$

where E_i means the CRB emissions for the ith pollutant (unit: g). $FRE_{j,t,m}$ represents the tth hourly FRE of the mth grid (2 km) in the jth region (unit: MJ). $EF_{i,j}$ represents the emission factors for the ith pollutant in the jth region (unit: g MJ^{-1}). All data were resampled into a 2 km × 2 km grid, which matched the spatial resolution of the NSMC-Himawari-8 fire product.

As shown in equation (2), FRP observations during the observation interval (1 h) were integrated to estimate FRE (assuming a flat FRP-emissions profile) in one fire pixel [40]:

$$FRE_{j,m} = FRP_{j,m} \times 60\ \text{min} \times 60\ \text{sec} \quad (2)$$

where $FRP_{j,m}$ represents the FRP of the mth grid in the jth region (unit: MW).

A reverse correction was required for the EFs of different pollutants based on the NSMC-Himawari-8 fire product [39]. To calculate accurate EFs based on VIIRS data, Xu et al. (2022) [39] built 63 regression models for historical pollutant emissions and the FRE to determine the relationship between combustion duration and peak FRP. Due to the system differences between VIIRS and Himawari-8/AHI, there is a fixed system bias in FRP for the same fire monitored by the two sensors. By counting the cumulative FRP of a large number of fires monitored by VIIRS and Himawari-8 from 2016 to 2019 across regions, we acquired our adjusted correction parameters (α) in equation (3), to calculate the FRE and EFs based on Himawari-8:

$$\alpha_j = \frac{FRP_{H,j}}{FRP_{V,j} - FRP_{H,j}} \quad (3)$$

where α_j stands for the correction coefficient. $FRP_{V,j}$ and $FRP_{H,j}$ stands for the cumulative FRP of VIIRS and Himawari-8 in the jth region, respectively (see Table S1).

Finally, EFs (as shown in Fig. S1) of different pollutants in each region based on NSMC-Himawari-8 fire product was obtained by adjusting the EFs calculated by Xu et al. (2022) [39] according to the correction coefficient in equation (4):

$$EF_{i,j} = \alpha_j \times EF\_Xu_{i,j} \quad (4)$$

where $EF\_Xu_{i,j}$ (see Table S2) represents the emission coefficients calculated by Xu et al. (2022) [39].

2.2.3. Calculation of day-night time

We utilized Python's Astral library (https://pypi.org/project/astral/) to calculate daily sunrise and sunset times for the region where the CRB occurred. Based on their respective locations and detected time, we could determine whether the CRB occurred during the daytime or nighttime. In cases where a CRB spanned two combustion stages, we assigned it to the stage with the longer duration. This approach could reveal the spatiotemporal distribution and their emissions of daytime and nighttime CRB, which has rarely been compared before.

2.2.4. Analysis of the lagging effects of CRB emissions on airborne pollutants

In general, pollutants emitted by biomass burning contribute approximately 9.7–55.5% [41] to the concentration of airborne pollutants, which is a relatively small and uncertain proportion compared to other sources such as industry and vehicle exhaust [2]. To identify the lagging effect of CRB emissions on airborne pollutants, it is key to select a region with a high number of CRB [42] so that the relative contribution of CRB can be highlighted. To this end, we chose Heilongjiang Province, a major grain-producing province with the highest annual amount of CRB in China [43,44], as the case study.

Previous studies show an approximate 1–3 days lagging effect between the CRB and the affected $PM_{2.5}$ concentration, based on the qualitative interpretation of the simultaneous variation trend of CRB and $PM_{2.5}$ concentration [9,45]. However, no quantitative evidence is available for determining a more precise description of the lagging effects of CRB on major airborne pollutants. Therefore, we first quantitatively determined the lagging effects of different pollutants emitted by CRB through correlation analysis. Specifically, we conducted a correlation analysis between the daily emissions of three pollutants emitted by CRB and the daily pollutant concentration data with different time lags (0, 1, 2, and 3 days later). The acquired correlation coefficients and significance levels provide a useful reference to determine the lagging effects of CRB on regional air quality.

3. Results

3.1. Spatiotemporal distributions of CRB

3.1.1. Diurnal variation

Based on the NSMC-Himawari-8 fire product, we revealed the hourly distribution pattern of CRB in China from 2019 to 2021. As shown in Fig. 1, the peak of CRB occurred at 18:00 in 2019, 20:00 in 2020, and 19:00 in 2021. Additionally, the daily number of CRB displayed a distinct skewed distribution, mainly concentrated between 17:00 and 20:00. Notably, the number of CRB spots within the 3 h accounted for 35.8% of the entire day, indicating that farmers had become more inclined to burn crop residue later in the day.

As shown in Fig. 2a, the total annual number of CRB spots consistently declined from 51,262 in 2019 to 28,773 by 2021. Specifically, the proportion of nighttime CRB across China in 2019, 2020, and 2021 was 51.9%, 48.5%, and 38%, respectively, indicating nighttime CRB, which exerted an even more severe emission influence, remained a major environmental issue. To our knowledge, no research has quantitatively revealed such a large proportion of nighttime CRB across China. Despite the lack of quantitative evidence, we could further presume that nighttime CRB across China could largely outnumber daytime CRB before 2019, majorly to avoid strict daytime environmental inspection. On the other hand, the simultaneous declining trend of the total number of CRB and the proportion of nighttime CRB from 2019 to 2021 suggested that environmental inspection, especially the increased nighttime inspection, had achieved notable effects on the management of CRB across China.

At the regional scale, as shown in Fig. 2b–h, we found that, except for the northeast, the number of daytime CRB was notably larger. The possible reason for this was that northeast China experienced a majority of CRB in China. Thus, the environmental inspection was the strictest here, leading to most daytime CRB moving to nighttime. As a comparison, CRB in other regions was not that intense, and thus, local inspection was relatively loose, leading to a larger proportion of daytime CRB. While a downward trend of

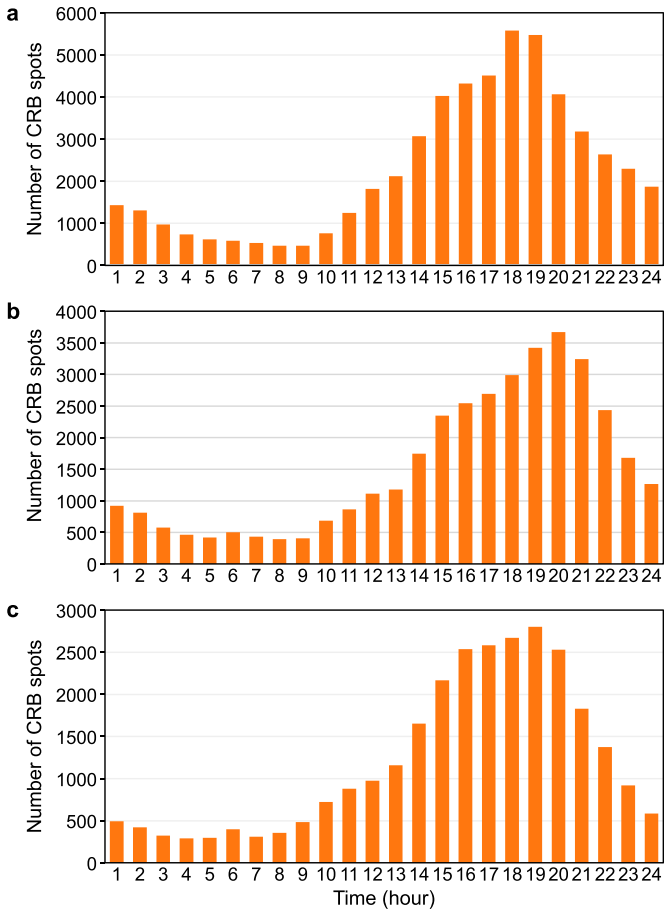

Fig. 1. The hourly distribution of CRB spots from 2019 (**a**), 2020 (**b**), and 2021 (**c**).

CRB (both daytime and nighttime) was maintained in most regions, and an unexpected increase of CRB was observed in eastern, southeastern, and southwestern China in 2020 or 2021, which required sufficient emphasis.

3.1.2. Seasonal variation

Fig. S2 presents the distribution of CRB density in different seasons, suggesting that CRB is primarily concentrated in spring (March–May) and winter (December–February). As explained above, farmers in China usually burn crop residues shortly after the autumn harvest, leading to severe local and even regional pollution episodes [46]. However, with the strict implementation of environmental inspection, especially in late autumn, they tended to postpone CRB to late winter (beyond the designated periods of burn prohibition) so that the common CRB peak in late autumn gradually shifted to winter across China.

In spring, most CRB was found in the northeast, particularly at the border of Heilongjiang, Jilin, and Nei Mongol. Many grid units (0.02°) exhibited a total number of fire spots exceeding 50, suggesting an extreme concentration. Additionally, the springtime CRB was also widely distributed in Yunnan, Sichuan, and Guizhou and mainly concentrated in March and April, as shown in Table S3, accounting for approximately 90–95% of total spring CRB. The primary purpose of CRB during this period was to clean the farm and kill pest eggs before spring plowing. Amongst the four seasons, the number of CRB spots was the lowest in summer, mainly aggregated in Henan, Shandong, and Jiangsu provinces, with most grid units containing CRB spots ranging from 1 to 10. In the past,

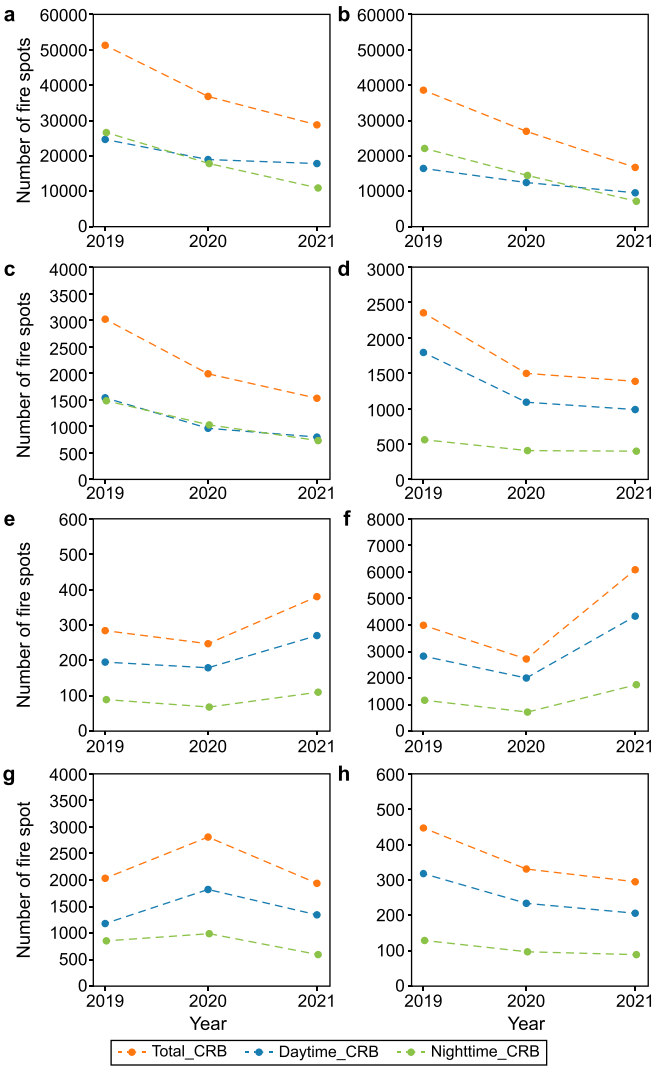

Fig. 2. The number of the total daytime and nighttime CRB spots in different regions: the whole China (**a**), the northeast (**b**), the north (**c**), the central (**d**), the east (**e**), the southeast (**f**), the southwest (**g**), and the northwest (**h**).

summer was a major period for CRB, particularly in provinces such as Shandong and Henan, where the maturation of the summer wheat harvest necessitated a rapid clearing for following agricultural practices. However, with the proliferation of comprehensive straw utilization techniques in these regions (the off-field utilization rate of crop straws reached 33.4%), the number of CRB has reduced significantly [47]. The number of CRB spots in autumn was significantly higher than in summer and was mainly concentrated in the northeast, followed by the southeast and central. This major CRB period coincided with the end of the national autumn harvest, with abundant crop residues. Although CRB was strictly prohibited during this period, some farmers secretly burned crop residues on farms. Winter CRB was mainly found in central and southern, with most grid units containing less than 20 CRB spots. As an exception, in winter 2019, CRB was highly concentrated in the northeast, accounting for approximately 70% of the national CRB in 2019. This extreme burning period may be primarily attributed to the delay of the autumn harvest burning period. Due to the stricter prohibition of CRB in the northeast in autumn, massive crop residues, which had not been processed promptly after the autumn harvest, were intensely burned in winter.

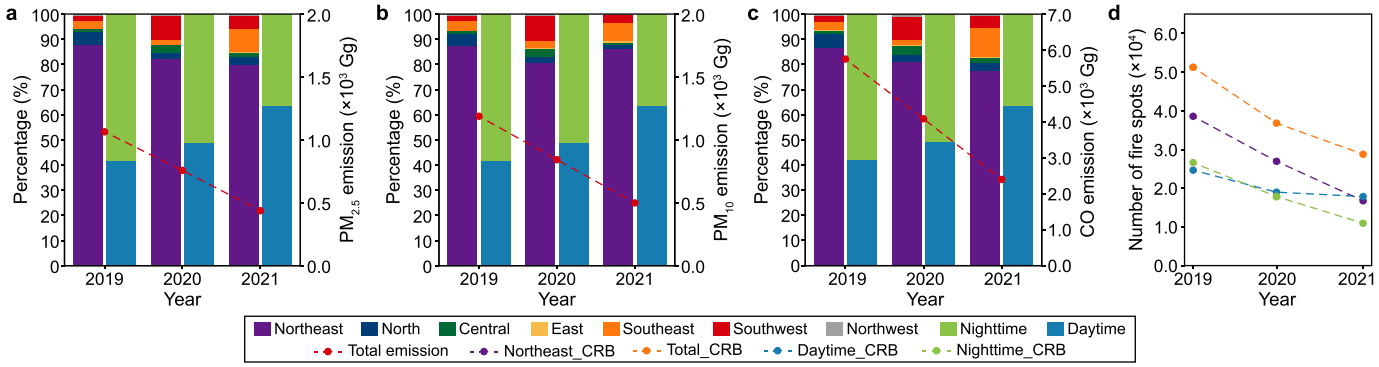

Fig. 3. The regional and diurnal variability in pollutants emitted by CRB. **a**–**c**, The regional and diurnal variations in the emission of $PM_{2.5}$ (**a**), PM_{10} (**b**), and CO (**c**) due to CRB combustion. The red dotted lines represent the total annual emissions of pollutants emitted by the corresponding CRB. **d**, The number of CRB spots nationally and in northeast China differentiated between nighttime and daytime occurrences.

Moreover, through the MEC and SDE analysis of CRB over the three years, we observed a distinct southward shift in the distribution center of CRB, particularly during the winter season, with the center moving on average 7.5 degrees southward annually. Fig. S3 displays the spatial variations of MEC and SDE of CRB from 2019 to 2021. The geographical location of MEC reflected the change in the distribution center of CRB, while the short axis and oblateness of SDE represented the distribution range and directionality of CRB, respectively. Overall, the directionality of CRB distribution in spring exhibited the strongest pattern, characterized by the highest flattening of SDE. The distribution range of CRB in autumn was the broadest. Between 2019 and 2021, the MEC of CRB in spring and summer was concentrated in Jilin and Henan provinces, respectively. In autumn, CRB demonstrated a slight southward shift, while in winter, the southward displacement of CRB was more pronounced, with an average annual southward shift of 7.5 degrees in the distribution center. The MEC and SDE analysis revealed that due to the strictest CRB restriction in northeast China, where CRB was most severe, CRB in northeast China reduced gradually, and the proportion of CRB in the southern part of China has increased notably in the past three years.

This suggests a change in the spatial distribution pattern of CRB across the country. Despite the still considerable proportion of CRB in the northeast region year-round, the concentration trend in this region has shown a declining sign. This is majorly attributed to the long-term implementation of strict CRB in this region.

3.2. Estimation of CRB emissions

Based on the calculated regional emission factors and fire radiative energy, we estimated the hourly emissions of three pollutants ($PM_{2.5}$, PM_{10}, and CO) caused by CRB in China from 2019 to 2021. As demonstrated in Table S4, total CO emissions were the highest among the three pollutants, reaching a cumulative emission of 12,236 Gg over the three years, followed by 2,530 Gg of PM_{10} and 2,258 Gg of $PM_{2.5}$. The overall emissions decreased significantly over the past three years, along with the decreased number of total CRB spots. Specifically, total $PM_{2.5}$ emissions for 2019, 2020, and 2021 were 1,064, 757, and 437 Gg, respectively. The total PM_{10} emissions for the same period were 1,188, 843, and 499 Gg, while CO emissions were 5,750, 4,087, and 2,399 Gg. The average annual reduction of the three pollutants was around 30%.

At the regional scale, we calculated the proportions of the three pollutants across major regions (seven areas). We found that emitted pollutants in northeast China took a dominant proportion in 2019, approximately 86.6% for $PM_{2.5}$, 87.8% for PM_{10}, and 87.5% for CO (Fig. 3). Although the proportions decreased annually, emissions in northeast China still accounted for 77.6% ($PM_{2.5}$), 80.0% (PM_{10}), and 77.9% (CO) in 2021. As shown in Fig. 3d, the number of CRB spots in the northeast constituted about 70% of the national CRB for three years, peaking at 75% in 2019. Meanwhile, CRB-induced emissions were also relatively large in the southeast and southwest, while the northwest contributed the lowest emissions.

From the diurnal perspective, over the three years, total nighttime CO, PM_{10}, and $PM_{2.5}$ emissions reached 6,262, 1,302, and 1,165 Gg, respectively (as shown in Table S4). During the daytime, total CO, PM_{10}, and $PM_{2.5}$ emissions reached 5,974, 1,227, and 1,092 Gg, respectively. While the total count of nighttime CRB spots (55,377) was notably smaller than that of daytime CRB (61,464), the total emission from nighttime CRB was 5% larger than that of daytime CRB. This suggested that due to the generally stagnant meteorological conditions at night [48], nighttime CRB causes more intense effects on local air quality [49]. Noticing this, China's monitoring of nighttime CRB has been enhanced accordingly. From 2019 to 2021, nighttime emissions of the three pollutants gradually decreased. In 2019, daytime emissions only contributed 42% of the total CRB emissions. By 2021, daytime emissions constituted 63% of the total emissions, suggesting the trend of secret nighttime CRB in China had been specifically controlled.

As shown in Table 1, from 2019 to 2021, the average amount of pollutants emitted per nighttime CRB was notably higher than that of daytime CRB. Specifically, each nighttime CRB was associated with more pollutant emissions compared to daytime CRB, higher than daytime CRB by approximately 2,170,209 g of $PM_{2.5}$, 2,324,995 g of PM_{10}, and 10,052,606 g of CO. However, this trend changed in 2021, when per nighttime CRB emission of the three pollutants was slightly less than per day CRB emissions by

Table 1
The airborne pollutants (unit: g $spot^{-1}$) emitted by each CRB.

Years	Pollutants	Daytime	Nighttime
2019	$PM_{2.5}$	18076121.65	23244189.38
	PM_{10}	20194677.48	25930163.06
	CO	98724691.61	124632392.47
2020	$PM_{2.5}$	19468425.83	21745343.98
	PM_{10}	21693063.54	24175604.77
	CO	105898217.17	116533956.26
2021	$PM_{2.5}$	15546395.42	14612038.25
	PM_{10}	17809280.30	16566240.72
	CO	85844332.27	79458711.32
Average	$PM_{2.5}$	17696980.97	19867190.54
	PM_{10}	19899007.11	22224002.85
	CO	96822413.68	106875020.02

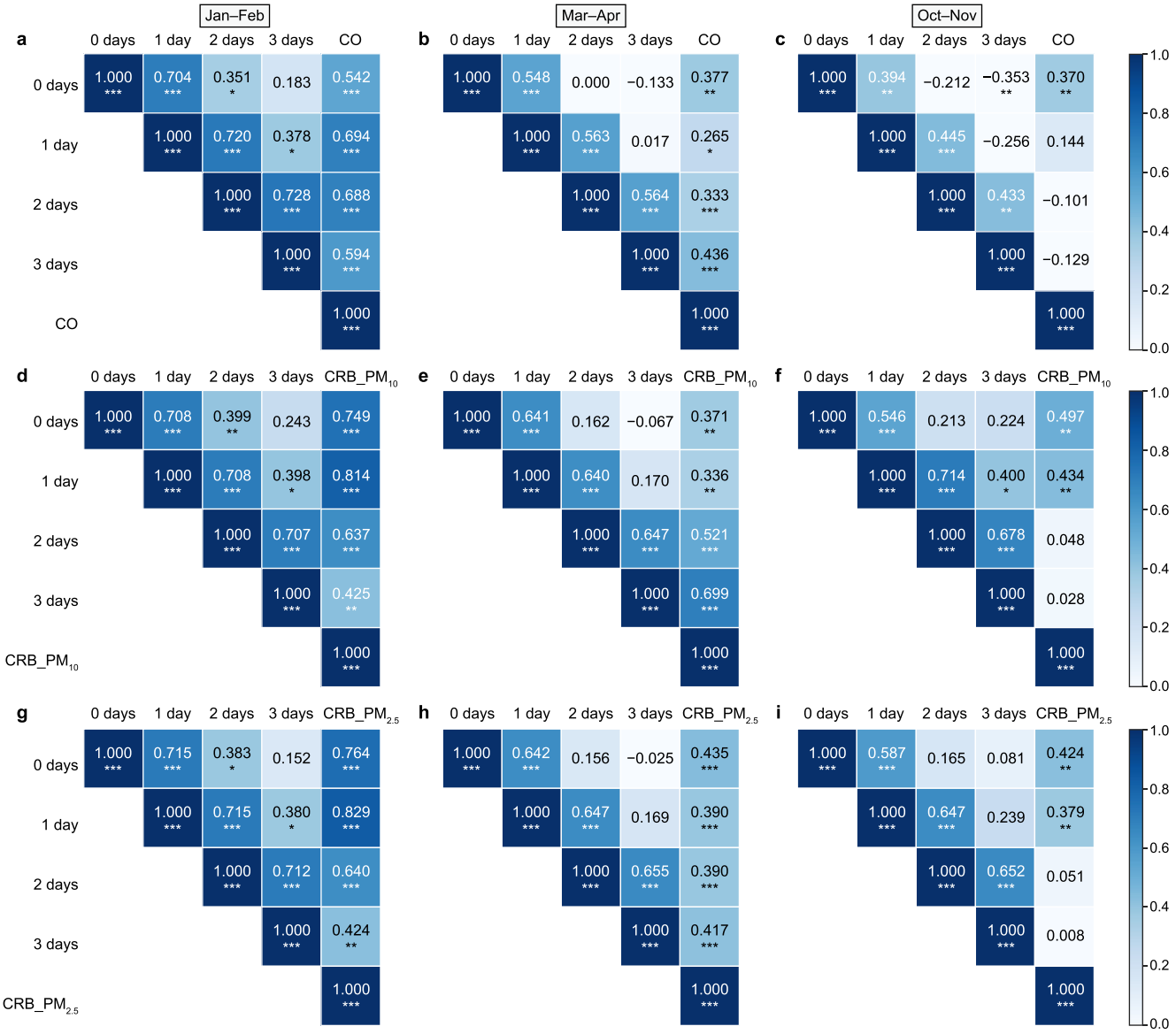

Fig. 4. The lagging times of three pollutants in three combustion periods. Each column in the figure represents different combustion periods, while each row denotes the lagging effect of a particular pollutant. The correlation matrix comprises five variables, including the concentrations of pollutants at four lagging times and the corresponding pollutant quantity emitted by CRB. **a**–**c**, The lagging effects of CO during Jan–Feb (**a**), Mar–Apr (**b**), and Oct–Nov (**c**). **d**–**f**, The lagging effects of PM_{10} during Jan–Feb (**d**), Mar–Apr (**e**), and Oct–Nov (**f**). **g**–**i**, The lagging effects of $PM_{2.5}$ during Jan–Feb (**g**), Mar–Apr (**h**), and Oct–Nov (**i**). Pearson correlations at different lagging times are shown in the correlation matrix: $^{*}P < 0.05$, $^{**}P < 0.01$, and $^{***}P < 0.001$. The final result is the average value after 10,000 bootstraps using the "block bootstrap" resampling technique.

approximately 934,357 g of $PM_{2.5}$, 1,243,040 g of PM_{10}, and 6,385,621 g of CO. We also conducted a monthly analysis of CRB emissions in 2021, as shown in Table S5, in April, when CRB was most concentrated throughout the year (accounting for approximately 37% of the total CRB spots), the nighttime emissions of the three pollutants were still significantly higher than daytime emissions.

To explore the causes of the difference between daytime and nighttime CRB emissions, we analyzed the average fire area and FRP information from the NSMC-Himawari-8 fire products, which were the major influencing factors for CRB emissions. While FRP for daytime CRB was usually larger than that of nighttime CRB due to stronger solar radiation and surface temperature [50], the average fire area per nighttime CRB was relatively larger due to such environmental factors as reduced fuel moisture, cooler temperatures, and radiation temperature inversions at night [51], which surpassed the impact of the lower FRP (Fig. S4). More importantly, due to generally loosened inspection in the nighttime, farmers were more likely to conduct CRB, while daytime CRB was secretly conducted at a smaller site. With stricter inspection in past years, not only the frequency but also the average area of nighttime CRB decreased notably, leading to the average fire area and emission per nighttime CRB being smaller than that of per daytime CRB in 2021.

In conclusion, with the increased awareness of the stronger influence of nighttime CRB, a growing emphasis has been placed on the reduction of nighttime CRB across China, which led to the reduced frequency and burning area of nighttime CRB, and thus, the mitigated influence of CRB on pollutant emissions.

3.3. Lagging effects of CRB on regional air quality

By analyzing the daily emissions of CRB-induced pollutants and the concentration of daily $PM_{2.5}$, PM_{10}, and CO in Heilongjiang province from 2019 to 2021, we calculated the correlation

coefficient between CRB and the concentration of daily $PM_{2.5}$, PM_{10}, and CO with the delay of 0, 1, 2 and 3 days during three concentrated CRB periods: January to February (winter), March to April (spring), and October to November (winter), to quantify the lagging effects of CRB on regional air quality.

As shown in Fig. 4, from January to February, the correlation coefficients between $PM_{2.5}$, PM_{10}, and CO emitted by CRB and regional pollutant concentration with the lag of one day were the largest, with R of 0.829 ($P < 0.001$), 0.81 ($P < 0.001$), and 0.69 ($P < 0.001$), respectively. From March to April, the correlation coefficients between CO and PM_{10} emitted by CRB and the pollutant concentration with the lag of three days were the highest, with R of 0.44 ($P < 0.001$) and 0.70 ($P < 0.001$), respectively. The correlation coefficient between $PM_{2.5}$ emitted by CRB and the pollutant concentration with the lag of 0 days was the highest, with R of 0.44 ($P < 0.001$). From October to November, the correlation coefficients between the three pollutants emitted by CRB and the pollutant concentration with the lag of 0 days were the highest, with R of 0.37 ($P < 0.01$), 0.50 ($P < 0.01$), and 0.42 ($P < 0.01$), respectively. Overall, the lagging effect of CRB was the strongest in the period between March and April and weakest in the period from October to November. The weak lagging effects of CRB emissions on $PM_{2.5}$ concentrations in late autumn suggested CRB emitted pollutants after the autumn harvest in the northeast region could be transported to a large region and explained why CRB after the autumn harvest immediately led to several regional and even national pollution episodes in 2015 and 2016 [52]. Yin et al. (2019) explored the sources of significant PM pollution events in northeast China in late 2015. Their detailed analysis using a Lagrangian transport model linked CRB in Heilongjiang Province directly to two major November smog events, providing theoretical support for our results.

The large variations of the lagging effects may be caused by the following reasons. Wind speed and temperature are primary influencing factors for the notable seasonal variations. Different from the strong wind in October and November, the wind speed in Heilongjiang in March and April, at around 2–3 levels, is much weaker than in other seasons [53], and not favorable for horizontal pollutant dispersion [54]. Concurrently, the ground temperature in Heilongjiang during this period remains very low at night, easily leading to the formation of nighttime temperature inversions and the limited dispersion of CRB-emitted pollutants [55,56]. These combined factors resulted in the notable lagging effect of CRB on regional air quality in March and April.

4. Discussion

4.1. Limitations and related studies

While this research provides a comprehensive and new understanding concerning the spatiotemporal variations of diurnal CRB and its environmental effects from 2019 to 2021 based on the new NSMC-Himawari-8 hourly fire product, some limitations remain. Firstly, due to sensor limitations, although Himawari-8 presented an extremely high-temporal resolution, its monitoring capability for small-scale fires was limited by its spatial resolution of 2 km [57]. Due to the missed identification of small CRB, the total amount of CRB and its related emissions remain underestimated. Secondly, the EFs for CO and PM were calculated based on laboratory data and statistical models from previous studies, which contain uncertainties [39]. The reduction of these uncertainties relies on the future availability of advanced fire products with hourly temporal resolution and improved spatial resolution.

We compared our emission estimation outputs in 2020 with some relevant studies [34,58], including GFEDv4.1s (Global Fire Emission Database, https://www.globalfiredata.org/), FINNv1.5 (NCAR Fire Inventory, https://www.acom.ucar.edu/Data/fire/), findings from Hong et al. (2022), and Xu et al. (2022). As shown in Fig. 5, the estimated CO emission in our study was 2.6 times that from GFEDv4.1s and 1.9 times that from FINNv1.5. Since these two global datasets mainly used MODIS daily global fire products, which led to massive missed CRB outside the overpass time [59], their results naturally presented severe underestimation. Conversely, outputs from Hong et al. (2022) and Xu et al. (2022) were 1.6 and 2.1 times our estimates, respectively. This was because their datasets were mainly based on VIIRS and JMA-Himawari-8 fire products, which included a substantial number of interference sources and thus caused a severe overestimation of CRB-induced emissions [60]. Despite a large inconsistency between these outputs, we can conclude that our estimation output lay in a reasonable range, given the resolution advantage and improved accuracy of NSMC-Himawari-8 fire products compared with MODIS and JMA fire products.

This study, spanning 2019 to 2021, identified three primary periods of CRB in China: spring, autumn, and late winter. There was a substantial shift in China's annual CRB pattern compared to before 2018, characterized by the disappearance of summer combustion periods and the emergence of late winter combustion periods [61]. Consistent with our result, Yin et al. (2021) found a sharp decline in the average FRP of CRB during the 2018 summer. Zhang et al. (2020) revealed a burning period (November–December) in late autumn and early winter from 2012 to 2015 [57], which may be caused by the strict implementation of residue-burning bans during the autumn post-harvest season. Our research indicates a further delay in this burning period to late winter (January–February), possibly due to a stricter burning ban. In addition, we found that CRB exhibited a southward shift trend, especially during winter. This shift was most pronounced in the winter, with an average annual southward shift of 7.5° in the distribution center. We also discovered that daily CRB was primarily concentrated in the evening (17:00–20:00), exhibiting a skewed distribution.

Previous studies suggested that $PM_{2.5}$ concentrations peak several days after the peak of CRB [9,42]. However, these investigations only analyzed the correlation between airborne pollutant concentrations and the number of CRB spots without attributing them to the CRB-induced emission of different pollutants and specifically identifying the difference in lagging effects across seasons and pollutants. Based on the NSMC-Himawari-8 fire product and the estimated CRB emissions, this research revealed that for Heilongjiang Province, where CRB was the most frequent and severe across China, the lagging effects of CRB on airborne pollutants was strongest in spring, and CRB was more likely to

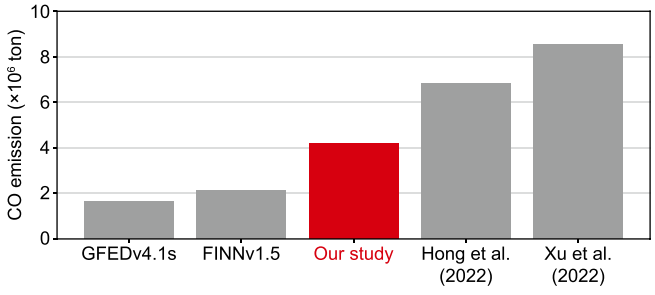

Fig. 5. Comparisons of CO emissions of CRB between other studies and this study. GFEDv4.1s and FINNv1.5 are based on MODIS fire products. Our study derives from the NSMC-Himawari-8 fire product. Outputs from Hong et al. (2022) [40] are based on the JMA-Himawari-8 fire product. Outputs from Xu et al. (2022) [39] are based on JMA-Himawari-8 and VIIRS fire products.

present immediate influence on regional air quality in late autumn. Meanwhile, the lagging effect of CRB on $PM_{2.5}$ concentrations was weakest, which explained why CRB in Heilongjiang Province used to cause regional or even national haze episodes.

4.2. Implementations

Given the more destructive potential of nighttime wildfires, our study investigated the diurnal differences in CRB emissions, which has rarely been investigated before. The results revealed that, on average, each nighttime CRB was associated with more pollutant emissions than daytime CRB, higher than daytime CRB by approximately 15 Gg of three pollutants ($PM_{2.5}$, PM_{10}, and CO). Moreover, our findings suggested that increased emissions from nighttime CRB resulted from a larger combustion area. With a stricter implementation of the CRB ban, the frequency and combustion area of nighttime CRB decreased significantly, making the average emission per nighttime CRB close to or even smaller than per daytime CRB. The recent variation of characteristics of nighttime CRB emissions in China highlighted the urgency and importance of all-day CRB inspections, especially during the late autumn, when CRB is more likely to further deteriorate already polluted air quality. This signals to regulators the necessity for leveraging geostationary satellites to enhance nighttime CRB regulation.

This research also highlighted changes in the spatiotemporal distribution of CRB. The significant southward shift of the CRB distribution center indirectly reflected a successful CRB control in northeast China, while future regulations of CRB in the south require further attention. Meanwhile, according to the skewed daily distribution of CRB, which is majorly concentrated between 18:00 and 20:00, increasing efforts should be placed on environmental inspection during this period.

Based on reliable hourly NSMC-Himawari-8 fire products and the estimation model for FRE and EFs, we calculated the total emissions of CRB in 2020. Compared with the outputs from GFEDv4.1s and FINNv1.5 based on daily or monthly sources, our estimation was much larger, suggesting CRB emissions could be largely underestimated with a daily frequency. Therefore, although this research did not provide a global estimation, it suggested that the existing global CRB emissions based on commonly employed global data sources GFEDv4.1s and FINNv1.5 were largely underestimated and should be further estimated based on the future availability of global hourly fire products.

4.3. Future work

To further address the underestimation of smaller fires, improved CRB identification may be achieved by the fusion of polar orbit satellites and geostationary satellites, including but not limited to Terra, Aqua, National Oceanic and Atmospheric Administration 20 (NOAA-20), FengYun-4A (FY-4A), FengYun-4B (FY−4B), and Himawari-8/9 satellites. This integration aims to comprehensively improve the spatiotemporal resolution to reduce omission errors of CRB. Meanwhile, due to the large variations in the meteorological conditions and crop types, EFs of CO and PM vary across regions. Presently, there is a lack of research focused on the region-specific calculation of EFs. Thus, estimating CRB emissions at the national scale based on the limited number of EFs inevitably contains uncertainties. To address this, field CRB experiments should be properly designed in a diversity of regions across China to fully consider the spatial variations of EFs of CRB emissions across China, and a comprehensive framework of EFs in different regions in China can be established. This combined strategy of fusing multiple satellite sources and refining emission factors can potentially provide a more comprehensive and accurate understanding of CRB-related airborne pollution.

5. Conclusion

The emissions of pollutants from CRB during the post-harvest and pre-planting periods profoundly impact air quality in China, constituting a significant source of atmospheric pollution and escalating the exposure risk for residents. Despite regulatory efforts leading to a gradual decline in CRB spots, tens of thousands of small and CRB events still occur annually. Moreover, the nocturnal barrier effect of burning activities in global climate change is progressively diminishing [62], potentially amplifying the hazards associated with nighttime CRB. Therefore, uncovering the spatiotemporal variations of CRB and elucidating the lagging effects of pollutant emissions hold crucial significance for targeted air quality management and enhancing the efficiency of CRB regulation.

In this study, we analyzed the spatiotemporal distribution of CRB in China from 2019 to 2021, using hourly NSMC-Himawari-8 fire products. We found that CRB primarily occurs during the later hours of the day, approximately between 18:00 and 20:00. Generally, the number of nighttime CRB spots has gradually decreased over time and has been lower than that of daytime CRB spots since 2020. Except for the northeast and northern regions, the remaining areas have consistently exhibited a higher frequency of daytime CRB than nighttime CRB over the past three years. Additionally, there has been a gradual weakening in the clustering trend of CRB incidents during this period. Although the northeast region remains the primary hotspot for CRB, its proportion has been decreasing annually, indicating a noticeable southward shift in the distribution center of CRB spots. In addition, we estimated the hourly emissions caused by CRB in China from 2019 to 2021. This analysis revealed that each nighttime CRB was associated with more pollutant emissions compared to daytime CRB, higher than daytime CRB by approximately 2,170,209 g of PM, 2,324,995 g of PM_{10}, and 10,052,606 g of CO, and the total emissions of CO, PM_{10} and $PM_{2.5}$ were 12,236, 2,530, and 2,258 Gg, respectively. Finally, our analysis of CRB emissions and CO and PM concentrations identified that the lagging effects of CRB on airborne pollutants were strongest in March and April, with a three-day lag of PM_{10} and CO ($P < 0.001$) and a zero-day lag of $PM_{2.5}$ ($P < 0.001$).

CRediT authorship contribution statement

Qiancheng Lv: Conceptualization, Investigation, Methodology, Software, Visualization, Writing - Original Draft, Writing - Review & Editing. **Zeyu Yang:** Investigation, Writing - Review & Editing. **Ziyue Chen:** Conceptualization, Writing - Review & Editing, Resources, Funding Acquisition. **Manchun Li:** Writing - Review & Editing. **Bingbo Gao:** Writing - Review & Editing. **Jing Yang:** Writing - Review & Editing. **Xiao Chen:** Writing - Review & Editing. **Bing Xu:** Writing - Review & Editing, Resources.

Declaration of competing interest

The authors declare that they have no known competing financial interests or personal relationships that could have appeared to influence the work reported in this paper.

Acknowledgment

This work was supported by the Open Research Program of the International Research Center of Big Data for Sustainable Development Goals (Grant No. CBAS2022ORP02) and the National Natural Science Foundation of China (Grant No.42171399).

Appendix A. Supplementary data

Supplementary data to this article can be found online at https://doi.org/10.1016/j.ese.2024.100394.

References

[1] Z. Cheng, S. Wang, X. Fu, J.G. Watson, J. Jiang, Q. Fu, C. Chen, B. Xu, J. Yu, J.C. Chow, J. Hao, Impact of biomass burning on haze pollution in the Yangtze River delta, China: a case study in summer 2011, Atmos. Chem. Phys. 14 (2014) 4573–4585.

[2] J. Chen, C. Li, Z. Ristovski, A. Milic, Y. Gu, M.S. Islam, S. Wang, J. Hao, H. Zhang, C. He, H. Guo, H. Fu, B. Miljevic, L. Morawska, P. Thai, Y.F. LAM, G. Pereira, A. Ding, X. Huang, U.C. Dumka, A review of biomass burning: emissions and impacts on air quality, health and climate in China, Sci. Total Environ. 579 (2017) 1000–1034.

[3] M. Cetin, H. Sevik, Change of air quality in kastamonu city in terms of particulate matter and CO2 amount, Oxid. Commun. 39 (2016) 3394–3401.

[4] J.D. Crounse, P.F. DeCarlo, D.R. Blake, L.K. Emmons, T.L. Campos, E.C. Apel, A.D. Clarke, A.J. Weinheimer, D.C. McCabe, R.J. Yokelson, J.L. Jimenez, P.O. Wennberg, Biomass burning and urban air pollution over the Central Mexican Plateau, Atmos. Chem. Phys. 9 (2009) 4929–4944.

[5] D.A. Permadi, N.T. Kim Oanh, Assessment of biomass open burning emissions in Indonesia and potential climate forcing impact, Atmos. Environ. 78 (2013) 250–258.

[6] J. Li, S.D. Xie, L.M. Zeng, L.Y. Li, Y.Q. Li, R.R. Wu, Characterization of ambient volatile organic compounds and their sources in Beijing, before, during, and after Asia-Pacific Economic Cooperation China 2014, Atmos. Chem. Phys. 15 (2015) 7945–7959.

[7] M. Cetin, A.K. Onac, H. Sevik, B. Sen, Temporal and regional change of some air pollution parameters in Bursa, Air Quality, Atmosphere & Health 12 (2019) 311–316.

[8] T. Ye, R. Xu, X. Yue, G. Chen, P. Yu, M.S.Z.S. Coêlho, P.H.N. Saldiva, M.J. Abramson, Y. Guo, S. Li, Short-term exposure to wildfire-related PM2.5 increases mortality risks and burdens in Brazil, Nat. Commun. 13 (2022) 7651.

[9] S. Yin, X. Wang, Y. Xiao, H. Tani, G. Zhong, Z. Sun, Study on spatial distribution of crop residue burning and PM2.5 change in China, Environ. Pollut. 220 (2017) 204–221.

[10] S. Sarkar, R.P. Singh, A. Chauhan, Increasing health threat to greater parts of India due to crop residue burning, Lancet Planet. Health 2 (2018) e327–e328.

[11] L. Huang, Y. Zhu, H. Liu, Y. Wang, D.T. Allen, M. Chel Gee Ooi, K. Manomaiphiboon, M. Talib Latif, A. Chan, L. Li, Assessing the contribution of open crop straw burning to ground-level ozone and associated health impacts in China and the effectiveness of straw burning bans, Environ. Int. 171 (2023) 107710.

[12] M. Uttreja, S.K. Ghosh, A. Krishnan, K. Lal, M. Sehgal, Assessment of the adverse effect of crop residue burning on respiratory health: a case study of Patiala, India, Lancet Planet. Health 6 (2022) S5.

[13] R. Lan, S.D. Eastham, T. Liu, L.K. Norford, S.R.H. Barrett, Air quality impacts of crop residue burning in India and mitigation alternatives, Nat. Commun. 13 (2022).

[14] G. He, T. Liu, M. Zhou, Straw burning, PM2.5, and death: evidence from China, J. Dev. Econ. 145 (2020) 102468.

[15] Z. Yuan, C.Z. Wu, H. Huang, G.F. Lin, Research and development on biomass energy in China, Int. J. Energy Technol. Pol. 1 (2002) 108.

[16] X. Huang, M. Li, J. Li, Y. Song, A high-resolution emission inventory of crop burning in fields in China based on MODIS Thermal Anomalies/Fire products, Atmos. Environ. 50 (2012) 9–15.

[17] M. Liu, Y. Song, H. Yao, Y. Kang, M. Li, X. Huang, M. Hu, Estimating emissions from agricultural fires in the North China Plain based on MODIS fire radiative power, Atmos. Environ. 112 (2015) 326–334.

[18] Y. Zhou, Y. Zhang, B. Zhao, J. Lang, X. Xia, D. Chen, S. Cheng, Estimating air pollutant emissions from crop residue open burning through a calculation of open burning proportion based on satellite-derived fire radiative energy, Environ. Pollut. 286 (2021) 117477.

[19] T. Li, Q. Dai, X. Bi, J. Wu, Y. Zhang, Y. Feng, Size distribution and chemical characteristics of particles from crop residue open burning in North China, J. Environ. Sci. 109 (2021) 66–76.

[20] Y. Liu, H. Zhao, G. Zhao, X. Zhang, A. Xiu, Carbonaceous gas and aerosol emissions from biomass burning in China from 2012 to 2021, J. Clean. Prod. 362 (2022) 132199.

[21] F. Li, X. Zhang, S. Kondragunta, C.C. Schmidt, C.D. Holmes, A preliminary evaluation of GOES-16 active fire product using Landsat-8 and VIIRS active fire data, and ground-based prescribed fire records, Remote Sens. Environ. 237 (2020) 111600.

[22] J. Cao, X. Peng, D. Xin, Feasibility study of prescribed burning for crop residues based on urban air quality assessment, J ENVIRON MANAGE 317 (2022) 115480.

[23] W. Xu, M.J. Wooster, T. Kaneko, J. He, T. Zhang, D. Fisher, Major advances in geostationary fire radiative power (FRP) retrieval over Asia and Australia stemming from use of Himarawi-8 AHI, Remote Sens. Environ. 193 (2017) 138–149.

[24] X. Lu, X. Zhang, F. Li, M.A. Cochrane, Improved estimation of fire particulate emissions using a combination of VIIRS and AHI data for Indonesia during 2015–2020, Remote Sens. Environ. 281 (2022) 113238.

[25] J. Chen, Q. Lv, S. Wu, Y. Zeng, M. Li, Z. Chen, E. Zhou, W. Zheng, C. Liu, X. Chen, J. Yang, B. Gao, An adapted hourly Himawari-8 fire product for China: principle, methodology and verification, Earth Syst. Sci. Data 15 (2023) 1911–1931.

[26] Y. Zhou, X. Xing, J. Lang, D. Chen, S. Cheng, L. Wei, X. Wei, C. Liu, A comprehensive biomass burning emission inventory with high spatial and temporal resolution in China, Atmos. Chem. Phys. 17 (2017) 2839–2864.

[27] H. Zheng, S. Cai, S. Wang, B. Zhao, X. Chang, J. Hao, Development of a unit-based industrial emission inventory in the Beijing–Tianjin–Hebei region and resulting improvement in air quality modeling, Atmos. Chem. Phys. 19 (2019) 3447–3462.

[28] Z. Klimont, D. Streets, Emission Inventories and Projections for Assessing Hemispheric or Intercontinental Transport, 2007.

[29] J. Peng, S. Chen, H. Lü, Y. Liu, J. Wu, Spatiotemporal patterns of remotely sensed PM2.5 concentration in China from 1999 to 2011, Remote Sens. Environ. 174 (2016) 109–121.

[30] T. Singh, A. Biswal, S. Mor, K. Ravindra, V. Singh, S. Mor, A high-resolution emission inventory of air pollutants from primary crop residue burning over Northern India based on VIIRS thermal anomalies, Environ. Pollut. 266 (2020) 115132.

[31] G. Roberts, M.J. Wooster, G.L.W. Perry, N. Drake, L.M. Rebelo, F. Dipotso, Retrieval of biomass combustion rates and totals from fire radiative power observations: application to southern Africa using geostationary SEVIRI imagery, J. Geophys. Res. 110 (2005).

[32] Y. Shen, C. Jiang, K.L. Chan, C. Hu, L. Yao, Estimation of field-level NOx emissions from crop residue burning using remote sensing data: a case study in hubei, China, Remote Sens-Basel 13 (2021) 404.

[33] S.F. Schreier, A. Richter, D. Schepaschenko, A. Shvidenko, A. Hilboll, J.P. Burrows, Differences in satellite-derived NOx emission factors between Eurasian and North American boreal forest fires, Atmos. Environ. 121 (2015) 55–65.

[34] G.R. van der Werf, J.T. Randerson, L. Giglio, T.T. van Leeuwen, Y. Chen, B.M. Rogers, M. Mu, M.J.E. van Marle, D.C. Morton, G.J. Collatz, R.J. Yokelson, P.S. Kasibhatla, Global fire emissions estimates during 1997–2016, Earth Syst. Sci. Data 9 (2017) 697–720.

[35] J. Wei, Z. Li, A. Lyapustin, L. Sun, Y. Peng, W. Xue, T. Su, M. Cribb, Reconstructing 1-km-resolution high-quality PM2.5 data records from 2000 to 2018 in China: spatiotemporal variations and policy implications, Remote Sens. Environ. 252 (2021) 112136.

[36] J. Wei, Z. Li, W. Xue, L. Sun, T. Fan, L. Liu, T. Su, M. Cribb, The ChinaHighPM10 dataset: generation, validation, and spatiotemporal variations from 2015 to 2019 across China, Environ. Int. 146 (2021) 106290.

[37] Y. Shi, T. Matsunaga, Y. Yamaguchi, Z. Li, X. Gu, X. Chen, Long-term trends and spatial patterns of satellite-retrieved PM2.5 concentrations in South and Southeast Asia from 1999 to 2014, Sci. Total Environ. 615 (2018) 177–186.

[38] H.A. Choukolaei, P. Ghasemi, F. Goodarzian, Evaluating the efficiency of relief centers in disaster and epidemic conditions using multi-criteria decision-making methods and GIS: a case study, Int. J. Disaster Risk Reduc. 85 (2023) 103512.

[39] Y. Xu, Z. Huang, J. Ou, G. Jia, L. Wu, H. Liu, M. Lu, M. Fan, J. Wei, L. Chen, J. Zheng, Near-real-time estimation of hourly open biomass burning emissions in China using multiple satellite retrievals, Sci. Total Environ. 817 (2022) 152777.

[40] X. Hong, C. Zhang, Y. Tian, H. Wu, Y. Zhu, C. Liu, Quantification and evaluation of atmospheric emissions from crop residue burning constrained by satellite observations in China during 2016–2020, Sci. Total Environ. 865 (2023) 161237.

[41] T. Ye, R. Xu, X. Yue, G. Chen, P. Yu, M.S.Z.S. Coêlho, P.H.N. Saldiva, M.J. Abramson, Y. Guo, S. Li, Short-term exposure to wildfire-related PM2.5 increases mortality risks and burdens in Brazil, Nat. Commun. 13 (2022) 7651.

[42] S. Cui, Z. Song, L. Zhang, Z. Shen, R. Hough, Z. Zhang, L. An, Q. Fu, Y. Zhao, Z. Jia, Spatial and temporal variations of open straw burning based on fire spots in northeast China from 2013 to 2017, Atmos. Environ. 244 (2021) 117962.

[43] G. Yang, H. Zhao, D.Q. Tong, A. Xiu, X. Zhang, C. Gao, Impacts of post-harvest open biomass burning and burning ban policy on severe haze in the Northeastern China, Sci. Total Environ. 716 (2020) 136517.

[44] H. Lu, Y. Chen, P. Zhang, H. Huan, H. Xie, H. Hu, Impacts of farmland size and benefit expectations on the utilization of straw resources: evidence from crop straw incorporation in China, SOIL USE MANAGE 38 (2022) 929–939.

[45] S. Yin, X. Wang, X. Zhang, Z. Zhang, Y. Xiao, H. Tani, Z. Sun, Exploring the effects of crop residue burning on local haze pollution in Northeast China using ground and satellite data, Atmos. Environ. 199 (2019) 189–201.

[46] X. Li, C. Zhang, P. Liu, J. Liu, Y. Zhang, C. Liu, Y. Mu, Significant influence of the intensive agricultural activities on atmospheric PM2.5 during autumn harvest seasons in a rural area of the North China Plain, Atmos. Environ. 241 (2020) 117844.

[47] M.O.A. MOA, Report on the Comprehensive Utilization of Crop Straw in China, 2022.

[48] F. Lestari, A. Adiwibowo, A. Kadir, N.A. Ramadhan, Validating the 6 year (2016–2021) anthropogenic induced small island wildfire hazards in Pulau Seribu archipelago, Indonesia, Prog Disaster Sci 14 (2022) 100236.

[49] P.H. Freeborn, W.M. Jolly, M.A. Cochrane, G. Roberts, Large wildfire driven increases in nighttime fire activity observed across CONUS from 2003–2020,

Remote Sens. Environ. 268 (2022) 112777.
[50] F. Di Giuseppe, S. Rémy, F. Pappenberger, F. Wetterhall, Using the Fire Weather Index (FWI) to improve the estimation of fire emissions from fire radiative power (FRP) observations, Atmos. Chem. Phys. 18 (2018) 5359–5370.
[51] G.J. Williamson, L.D. Prior, W.M. Jolly, M.A. Cochrane, B.P. Murphy, D.M.J.S. Bowman, Measurement of inter- and intra-annual variability of landscape fire activity at a continental scale: the Australian case, Environ. Res. Lett. 11 (2016) 35003.
[52] X. Long, X. Tie, J. Cao, R. Huang, T. Feng, N. Li, S. Zhao, J. Tian, G. Li, Q. Zhang, Impact of crop field burning and mountains on heavy haze in the North China Plain: a case study, Atmos. Chem. Phys. 16 (2016) 9675–9691.
[53] Z. Li, Z. Xiao, C. Zheng, Observation analysis of wind climate in China for 1971–2017 under the demand of wind energy evaluation and utilization, Energy Rep. 7 (2021) 3535–3546.
[54] S. Gautam, C. Sammuel, A. Bhardwaj, Z. Shams Esfandabadi, M. Santosh, A.S. Gautam, A. Joshi, A. Justin, G.J. John Wessley, E.J. James, Vertical profiling of atmospheric air pollutants in rural India: a case study on particulate matter (PM10/PM2.5/PM1), carbon dioxide, and formaldehyde, Measurement 185 (2021) 110061.
[55] P.D. Hien, P.D. Loc, N.V. Dao, Air pollution episodes associated with East Asian winter monsoons, Sci. Total Environ. 409 (2011) 5063–5068.
[56] B. Liu, X. Ma, Y. Ma, H. Li, S. Jin, R. Fan, W. Gong, The relationship between atmospheric boundary layer and temperature inversion layer and their aerosol capture capabilities, Atmos. Res. 271 (2022) 106121.
[57] T. Zhang, M.C. de Jong, M.J. Wooster, W. Xu, L. Wang, Trends in eastern China agricultural fire emissions derived from a combination of geostationary (Himawari) and polar (VIIRS) orbiter fire radiative power products, Atmos. Chem. Phys. 20 (2020) 10687–10705.
[58] C. Wiedinmyer, S.K. Akagi, R.J. Yokelson, L.K. Emmons, J.A. Al-Saadi, J.J. Orlando, A.J. Soja, The Fire INventory from NCAR (FINN): a high resolution global model to estimate the emissions from open burning, Geosci. Model Dev. (GMD) 4 (2011) 625–641.
[59] X. Qiu, L. Duan, F. Chai, S. Wang, Q. Yu, S. Wang, Deriving high-resolution emission inventory of open biomass burning in China based on satellite observations, Environ. Sci. Technol. 50 (2016) 11779–11786.
[60] W. Schroeder, P. Oliva, L. Giglio, I.A. Csiszar, The New VIIRS 375m active fire detection data product: algorithm description and initial assessment, Remote Sens. Environ. 143 (2014) 85–96.
[61] S. Yin, M. Guo, X. Wang, H. Yamamoto, W. Ou, Spatiotemporal variation and distribution characteristics of crop residue burning in China from 2001 to 2018, Environ. Pollut. 268 (2021) 115849.
[62] J.K. Balch, J.T. Abatzoglou, M.B. Joseph, M.J. Koontz, A.L. Mahood, J. McGlinchy, M.E. Cattau, A.P. Williams, Warming weakens the night-time barrier to global fire, Nature 602 (2022) 442–448.